HHS Public Access

Author manuscript

Chemphyschem. Author manuscript; available in PMC 2022 January 24.

Published in final edited form as:

Chemphyschem. 2021 December 13; 22(24): 2526–2534. doi:10.1002/cphc.202100667.

A Versatile Compact Parahydrogen Membrane Reactor

Patrick M. TomHon[†,a], **Suyong Han**[†,b], **Sören Lehmkuhl**[a], **Stephan Appelt**[c,d], **Eduard Y. Chekmenev**[e,f], **Milad Abolhasani**[b], **Thomas Theis**[a,g,h]

[a]Department of Chemistry, North Carolina State University, Raleigh, NC, 27695, United States

[b]Department of Chemical and Biomolecular Engineering, North Carolina State University, Raleigh, NC, 27606, United States

[c]Central Institute for Engineering, Electronics and Analytics – Electronic Systems (ZEA-2), Forschungszentrum Jülich GmbH, D-52425 Jülich, Germany

[d]Institut für Technische Chemie und Makromolekulare Chemie (ITMC), RWTH Aachen University, D-52056 Aachen, Germany

[e]Department of Chemistry, Integrative Biosciences (Ibio), Karmanos Cancer Institute (KCI), Wayne State University, Detroit, MI, 48202, United States

[f]Russian Academy of Sciences, Leninskiy Prospekt 14, 119991 Moscow, Russia

[g]Joint Department of Biomedical Engineering, University of North Carolina, Chapel Hill and North Carolina State University, Chapel Hill, NC and Raleigh, NC, United States

[h]Department of Physics, North Carolina State University, Raleigh, NC, 27695, United States

Abstract

We introduce a Spin Transfer Automated Reactor (STAR) that produces continuous parahydrogen induced polarization (PHIP), which is stable for hours to days. We use the PHIP variant called signal amplification by reversible exchange (SABRE), which is particularly well suited to produce continuous hyperpolarization. The STAR is operated in conjunction with benchtop (1.1 T), and high field (9.4 T) NMR magnets, highlighting the versatility of this system to operate with any NMR or MRI system. The STAR uses semipermeable membranes to efficiently deliver parahydrogen into solutions at nano to milli Tesla fields, which enables ^{1}H, ^{13}C and ^{15}N hyperpolarization on a large range of substrates including drugs and metabolites. The unique features of the STAR are leveraged for important applications, including continuous hyperpolarization of metabolites, desirable for examining steady-state metabolism in vivo as well as for continuous RASER signals desirable for the investigation of new physics.

Graphical Abstract

pmtomhon@ncsu.edu, ttheis@ncsu.edu.

[†]These authors contributed equally.

Supporting information for this article is given via a link at the end of the document.

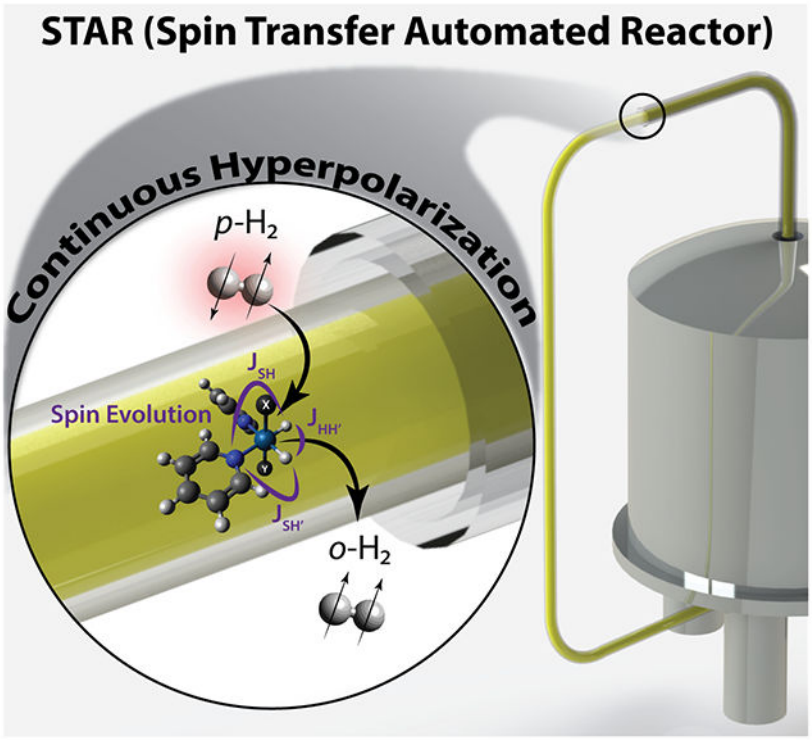

The spin transfer automated reactor (STAR) system is a next-generation continuous microfluidic system for generation of hyperpolarized substrates with parahydrogen-based chemistry. In the present work, we demonstrate continuous production of hyperpolarized biomedically relevant compounds (pyruvate and metronidazole) and push the boundaries of new parahydrogen-driven RASER physics with continuous pumping of a hyperpolarized solution.

Keywords

Hyperpolarization; parahydrogen; NMR; fluidics; RASER

Introduction

Nuclear magnetic resonance (NMR) and Magnetic Resonance Imaging (MRI) are invaluable tools to provide a wealth of chemical, structural, and spatial information. Traditional NMR and MRI are limited by low thermal spin polarization, limiting sensitivity, and requiring large superconducting magnets for spectroscopy and imaging. Hyperpolarization methods overcome these sensitivity limitations by redistributing nuclear spin populations from their thermal equilibrium [1,2]. Generally, hyperpolarization methods utilize an external, highly polarized spin source such as electrons [3] or vaporized alkali metals [4] and their polarization is transferred to nuclear spins. Parahydrogen-induced hyperpolarization (PHIP) [5,6] uses parahydrogen (*p*-H2) as a source of spin order and generates hyperpolarization in target substrates either through chemical addition [5] or exchange reactions [7]. Hydrogenation reactions allow for direct incorporation of p-H_2 into the target substrate but are more limited in their scope as they require chemical modification [8]. A relatively

new non-hydrogenative variant of PHIP, Signal Amplification By Reversible Exchange (SABRE) is a p-H_2 based method that uses reversible reactions of an organometallic catalyst to transfer spin order from p-H_2 to target substrates [7,9]. SABRE hyperpolarization works for a growing range of substrates [10], and can be generated quickly, cheaply, continuously, and repeatedly. Figure 1 illustrates how SABRE uses the reversible exchange reactions of parahydrogen (p-H_2) and substrate on a polarization transfer complex (PTC). Figure 1 also indicates how optimization of p-H_2 delivery in this biphasic, gas-liquid, system is crucial for maximizing hyperpolarization as it requires efficient continuous refreshment of p-H_2. Standard gas delivery methods include bubbling and shaking to mix gas and liquid phases [11,12], but these suffer from poor, uncontrolled, and irreproducible mass transfer of hydrogen. Moreover, continuous and steady delivery of hyperpolarized (HP) substrate in solution for hours to days is desirable for many applications (see SI section 10), such as the study of steady-state metabolism and precision measurements with long acquisition times as demonstrated here. In contrast to single-shot batch hyperpolarization experiments, continuous hyperpolarization can act as a reemerging source of polarization in analogy to the T_1 regeneration of longitudinal magnetization in a standard NMR experiment. This feature enables standard multiscan and multidimensional NMR experiments, *e.g.,* HSQC, NOESY, etc. with hyperpolarization. To address limitations of existing approaches [13–16], we advance the use of hollow membranes in our Spin Transfer Automated Reactor (STAR), which features negligible solvent evaporation and enables continuous and automatic operation for days.

To circumvent the mass transfer limitation of conventional gas delivery methods using batch reactors, we utilize a highly gas-permeable tubular membrane in a tube-in-tube configuration, previously used to enhance gas-liquid reactions [17–19]. Conventional batch methods such as bubble columns offer relatively low gas-liquid interfacial area (50-600 m^2/m^3) [20,21]. Due to the poorly defined specific interfacial area, reactions often suffer mass-transfer limitations by low overall mass transfer coefficients of the reactor (0.005-0.25 s^{-1}) [22]. Utilizing Teflon AF-2400 tubing in the tube-in-tube flow reactor configuration, significantly higher specific interfacial area of ~5000 m^2/m^3 is achieved, which increases the mass transfer rate of hydrogen into the SABRE system to 0.1-1 s^{-1} [17]. Figure 2 illustrates the Spin Transfer Automated Reactor (STAR) for p-H_2 hyperpolarization, which maximizes p-H_2 delivery through a tube-in-tube flow reactor. Additionally, the compact design of the membrane reactor allows for an applied polarization transfer field (B_p) in any magnetic field (from nT to mT) and can be utilized in conjunction with high- (multi-Tesla) and low-field NMR/MRI magnets (sub-Tesla).

In turn we obtain a platform with the developed chemistry to hyperpolarize virtually any nucleus [10,23,24] that can be coupled to any NMR or MRI detection system. In this paper, we demonstrate this general versatility with a few combinations of hyperpolarized nuclei (^1H, ^{15}N, ^{13}C) with detection in benchtop (1.1 T permanent magnet) and traditional (9.4 T super conducting) NMR. We show that the STAR is capable of nearing SABRE hyperpolarization levels achievable only in single shot bubbling experiments.

Two currently emerging applications from the field of parahydrogen-induced polarization are *in vivo* imaging of hyperpolarized metabolites [6,25–27] and exploration of new physics

governing RASER (radio frequency amplification by stimulated emission of radiation). Here, we demonstrate and discuss the STAR utility for these two applications: a) simplifying hyperpolarization to continuously produce HP contrast agents, metronidazole and pyruvate, which are potential metabolic imaging probes for hypoxia [28,29] and cancer cell metabolism [30,31], respectively.; and b) continuous RASER effects, which are expected to have significant applications in precision measurements and quantum information science [32,33]. Both metabolite production and RASER effects are detected at two different magnetic fields (1 T and 9.4 T).

Results and Discussion

The developed STAR technology equipped with a compact tube-in-tube flow reactor and computer-controlled fluid handling systems are shown in Fig. 2. The sample solution is pumped through the inner annulus of the tube-in-tube reactor, while gas is delivered through the outer annulus of the reactor. The tube-in-tube flow reactor offers one of the highest commercially available hydrogen gas permeabilities [19,34], ensuring intensified hydrogen delivery and subsequent removal in the STAR system. Here, hydrogen gas delivery for hyperpolarization is conducted in the first tube-in-tube flow reactor, shown at the bottom of the fluid path in Fig. 2, while partial removal of hydrogen gas occurs in the second tube-in-tube flow reactor shown at the top of the fluidic path. Extensive studies are required to correctly model and predict the gas flux in this paired flow reactor configuration, however we show in the Supplementary Information (SI) that the degassing stage does increase the attained hyperpolarization measurably. Existing work documents the efficiency of delivery [17] and removal [35] of hydrogen gas with Teflon AF 2400 membranes.

The flow reactor used in the construction of this device is wrapped into a compact coil, enabling easy coupling with a solenoid and/or magnetic shield around the reactor for easy control of the polarization transfer field, B_{pol}. For proton SABRE hyperpolarization we use a home-built solenoid (S.I. section 2.1) to control milli-Tesla magnetic fields throughout the reactor. This field corresponds to the matching condition of aligning the J-coupling and frequency difference of the p-H_2 derived hydrides and target protons (ca. 32 ppm) [36,37]. While standard SABRE proton hyperpolarization utilizes mT magnetic fields, this method can be adapted to hyperpolarization of spin-½ heteronuclei (*e.g.,* ^{15}N, ^{13}C) by application of μT fields for the polarization transfer process. The difference in field (μT vs mT) arises from the large frequency difference given by the disparate gyromagnetic ratios of the hydrides and target heteronuclei (vs. the frequency difference between hydrides and target protons given in ppm). The heteronuclear frequency difference is minimized at μT fields, created by magnetic shielding and fine-tuned with a small solenoid to meet the J-coupling and frequency difference matching condition described above [24,36]. This method is termed SABRE-SHEATH (Shield Enables Alignment Transfer to Heteronuclei) [36,38].

As seen in Fig. 2, the solution enters a closed fluidic loop with a secondary reservoir to ensure that the entire fluidic path is filled with fluid during system operation. The solution is polarized in the fluidic path as it flows through the primary hydrogen flow reactor, where p-H_2 can saturate the solution and diffuse through the liquid phase to arrive at the catalytic centers. Within the hydrogen flow reactor, the p-H_2 is consumed and converted

to orthohydrogen, which is then free to diffuse and exchange with fresh *p*-H_2. The HP substrate can be collected in volumetric fractions or detected continuously. After detection, the solution is recycled through a secondary flow reactor, operated with inert gas (e.g., N_2, Ar) to decrease the concentration of H_2 in the solution. In the secondary flow reactor, the inert gas flows at a reduced pressure relative to the liquid phase (ΔP = 10–20 psi), decreasing the concentration of H_2 in the solution. This concentration decrease enables a fast saturation of fresh *p*-H_2 when the solution recycles into the primary hydrogen reactor.

For polarization transfer with SABRE we use the standard iridium-IMes polarization transfer catalyst [IrCl(COD)(IMes)]; COD = 1,5-cyclooctadiene; IMes =1,3-bis(2,4,6-trimethylphenyl)-imidazol-2-ylidene] [10,39] in methanol-d_4 and several target substrates. First, as shown in Fig. 3, we analyse results with pyridine (**1**) and pyrazine (**2**). For these compounds, polarization was carried out at B_{pol} = 6.5 ± 0.1 mT (S.I. Section 2.1 for details). We obtain a signal enhancement of 3130 for pyridine (**1**) and 3600-fold on pyrazine (**2**) over a thermal measurement at 1.1 T (Magritek 43 MHz Spinsolve), corresponding to polarizations of 1.18% and 1.35% respectively. Figure 3 contains overlays of the 1.1 T thermalized spectra (red) and hyperpolarized spectra (blue) for both pyridine (**1**) (Fig. 3(a)) and pyrazine **(2)** (Fig. 3(b)).

Notably, the measurements above do not directly reflect polarization levels obtained in the flow reactor itself but incorporate the relaxation during the transfer period of the hyperpolarized solution from the flow reactor to the sensitive volume of the benchtop 1.1 T NMR magnet. The transfer period is 8.7 s at a flow rate of 2.0 mL/min. Hence the observed polarization (P_{obs}) is determined by $P_{obs} = P \times (1/e)^{T_t/T_1}$, where P is the initial polarization level, T_t is the transfer period, and T_1 is the longitudinal relaxation time constant. We measured T_1 = 5.9 s at 1.1 T of the protons of **(2)** (see SI Section 4.1). Accordingly, we estimate that polarization P_{1H} = 5.9% was achieved in the reactor. A further critical question is whether the polarization was able to reach an equilibrated steady state by the time the solution leaves the reactor. For **(2)** with a buildup time constant T_b = 3.7 ± 0.9 s, polarization is fully accumulated with a given reactor retention time of 13.2 s at 2.0 mL/min. For pyridine **(1),** We observe a similar transfer relaxation effect as for (**2**), however, the buildup of hyperpolarization on **(1)** is slower with T_b = 18 ± 3 s, therefore accumulating only 43% of maximum polarization.

STAR SABRE-SHEATH Hyperpolarization of [$^{15}N_3$] Metronidazole.

Hyperpolarization of biologically relevant compounds, such as the common and FDA-approved antibiotic metronidazole, is of interest for both *in vivo* pre-clinical and clinical studies to elucidate disease-associated metabolic changes and disruptions. For example, metronidazole has potential as a probe for hypoxia sensing, mirroring the current implementation of ^{18}F-fluoromisonidazole (FMISO) in positron emission tomography (PET) imaging [40]. Metronidazole is also of interest due to its high relative polarization and long relaxation times, ^{15}N T_1 = 9.7 min [41,42].

Demonstrating the utility of the STAR in conjunction with other instruments, we measure with a high-field (9.4 T) magnet. For this purpose, we designed a top-access flow probe

using a high-pressure NMR. A diagram of the adapted detection apparatus is shown in SI section 5. We use this setup to showcase both continuous detection of hyperpolarization in a superconducting NMR magnet, and continuous ^{15}N SABRE-SHEATH on a biologically relevant molecule. The spectra in Fig. 4 correspond to the acquisition of continuously HP [$^{15}N_3$] metronidazole at 9.4 T. We optimized the flow rate and demonstrated a maximum polarization at 2.0 mL/min (Details in section 7.2 of the S.I). Using the STAR system, we achieve ~1.4 times higher polarization than with bubbling when the parahydrogen mixing time is matched in the bubbling and reactor experiments (See inset Table in Fig. 4. The details of the comparison are in SI section 7.3). However, we point out that the steady-state polarization observed in the reactor on metronidazole after several tens of minutes of operation time is ~80% lower than the initial maximum polarization observed after 5 to 10 minutes of operation (See SI section 7.4). This finding clearly indicates that further optimization may increase steady-state polarization, therefore and we are continuing to engineer solutions to ortho/para-hydrogen exchange, to enable maximum re-dissolution of fresh parahydrogen into solution during steady-state operation.

Continuous ^1H SABRE has been detected at high field previously [13,14], the current demonstration with the STAR system is the first continuous SABRE-SHEATH implementation. Continuous pumping of HP solution through the NMR tube eliminates recycle delays enabling fast averaging to build additional SNR quickly in any NMR experiment and gives access to any standard multidimensional experiment. For example, operation of the STAR system at 2.0 mL/min with a sensitive volume retention time of 3.0 s enables 600 scans for every 30 min period ($\sqrt{600} \approx 24$ fold SNR gain over single-shot hyperpolarized experiments). In addition, continuous production of a HP substrates like metronidazole promises *in vivo* explorations by tapping HP solution off the continuously cycling reactor system, for example to measure steady-state metabolism. As we discuss next, continuous heteronuclear polarization with STAR SABRE-SHEATH can also be expanded to ^{13}C hyperpolarization on well-known contrast agents such as ^{13}C-labeled pyruvate.

STAR SABRE-SHEATH Hyperpolarization of Pyruvate.

Recent work in the field of SABRE hyperpolarization has significantly broadened the substrate scope beyond traditional nitrogen heterocycles to include carboxylates and structurally related substrates including acetate [43] and pyruvate [44,45]. These substrates are enabled through introduction of a sulfoxide co-ligand such as methyl sulfoxide or methyl phenyl sulfoxide to allow for dynamic exchange of both the hydride and substrate on the iridium center [44–46]. Importantly, this new chemistry enables SABRE hyperpolarization of pyruvate, a common biomolecule in cell energy metabolism [25,27]. For example, imaging of pyruvate metabolism *in vivo* enables rapid detection of cancer cell metabolism via the Warburg effect promising early cancer diagnosis and monitoring of ongoing cancer therapies [25,26,31].

Continuous SABRE-SHEATH driven polarization of pyruvate provides a new opportunity in contrast to other *p*-H_2 [47,48] or dynamic nuclear polarization (DNP) based [49] methods, as SABRE can easily produce a continuous stream of hyperpolarized media. In addition, utilization of the singlet spin order on parahydrogen allows for generation of a singlet spin

state on the two ^{13}C nuclei of $^{13}C_2$-pyruvate. As indicated in Figure 5, we demonstrate large volume continuous production of hyperpolarized $^{13}C_2$-pyruvate, using SABRE-SHEATH in the STAR system. Currently, the observed maximum polarization in our benchtop NMR with the STAR system is 0.20%. This is less than the maximum polarization on $^{13}C_2$-pyruvate of 0.71% when we use a bubbling method of p-H_2 mixing (Table, Fig. 5). This is a result of insufficient retention time in the current flow reactor. The 0.20% ^{13}C polarization levels were achieved with a 13.1 s retention time in the reactor at 2 mL/min. However, the buildup rate constant is T_b (1-^{13}C) ≈ 34 ± 5 s for pyruvate hyperpolarized at 0.8 μT (see SI section 4.3 for full details). We note that pyruvate has a strong magnetic field dependence in the μT regime. Therefore, we were not able to implement the same scaled-up flow reactor as for metronidazole because of the difference in homogeneity requirements of the polarization transfer fields for metronidazole vs. pyruvate, where the B_{pol} dependence of metronidazole broader relative to that of pyruvate. The details of this comparison are described in SI section 3.2.

As the singlet state hyperpolarized in pyruvate has a relatively long relaxation time T_s = 85.4 ± 8.5 s [45] relative to the transfer time T_t = 8.7 s, relaxation does not significantly impact the observed ^{13}C polarization. Accounting for the insufficient buildup time in this first-generation reactor, the expected polarization with a hypothetical, larger reactor with sufficient field homogeneity and a retention time of 65 s is 0.7%, corresponding to the maximum polarization achieved with our bubbling method of parahydrogen mixing.

The SABRE-STAR RASER.

The p-H_2 pumped RASER (Radiowave Amplification by Stimulated Emission of Radiation), was first reported in 2017 [32] and displays unexplored physics in the field of magnetic resonance. Unlike ^{129}Xe or ^3He SEOP-based Masers [50], the p-H_2 pumped RASER can explore spin-spin interactions (J-couplings) inside molecules and chemical shift differences with unprecedented precision [33,51]. In some respects, the RASER is a magnetic resonance analogue to a LASER, which operates at typical frequencies of 10^{14} – 10^{15} Hz. Like the LASER, the RASER also requires a pumped population inversion that can give way to coherent emission of radiation. However, unlike the LASER, the p-H_2 pumped RASER, drives stimulated emission at frequencies of kHz to MHz [32,33,52]. Continuous pumping of population inversion within nuclear spin states, while coupled to an LC NMR circuit enables continuous detection of NMR signal without decay, enabling measurement of NMR signals with arbitrarily narrow lines, thereby accessing a range of applications, including high-precision magnetometry down to the μHz level [32]. Subsequent publications have explored the p-H_2 pumped RASER effects in more detail. A problem that becomes apparent in this work is that bubbling of p-H_2 through the solutions creates susceptibility artifacts, which are prone to destroy the RASER effect or limit its lifetime. [32,51,53] Susceptibility artifacts from bubbling are minimized at low magnetic fields (e.g. in the mT regime), but cause much greater challenges as parahydrogen RASER's are implemented on typical NMR systems with field strengths of several Tesla [32,51,53]. In this work, we use the STAR system to demonstrate SABRE-pumped RASER effects at higher magnetic fields (1.1 T and 9.4T), resulting in continuous detection of RASER signals on the timescale of minutes to hours without the otherwise hampering susceptibility artifacts induced by bubbling.

A schematic of the basic RASER operation is shown in Fig. 6(a). Here, population inversion is pumped by SABRE in the STAR and introduced to an NMR LC resonant circuit. If the population inversion is above the so-called RASER threshold, the RASER effect is enabled by back-action of the LC-circuit on the nuclear spins. The polarization threshold of a RASER system is given by,

$$d_{th} = \frac{-4}{\mu_0 \eta \hbar \gamma^2 T_2^* Q n_S} \quad \text{(Eq.1)}$$

Where d_{th} is the population inversion at the RASER threshold, μ_0 is the vacuum permeability, η is the filling factor of the coil, γ is the gyromagnetic ratio of the target spins, T_2* is the effective transverse relaxation time, Q is the quality factor of the LC resonator, and n_s is the number of spins in the sample [33].

For the RASER as described previously [32,33], it is critical that the relaxation rates of the nuclear spins are long relative to the fast decay rate of the photons in the resonator [33]. Early iterations of these RASER demonstrations relied on high-quality-factor enhanced (EHQE) or cryo-enhanced inductive NMR detectors (Q>300) to generate strong interactions between the highly polarized solution and the coil [32,53], but more recent work demonstrated that RASER signals can even be detected in benchtop NMR spectrometers with quality factors below 100 with a sufficient population inversion [51]. Here we expand on these single shot experiments that were achieved with hydrogenative PHIP and demonstrate continuous detection of *p*-H_2 RASER effects pumped with our new SABRE-STAR system within a 1.1 T benchtop NMR.

In Fig. 6(b), we show RASER effects during the buildup of polarization on pyrazine protons. Polarization builds up slowly as the pressure is gradually ramped from 0 to 90 psi in the reactor. During this pressurization hyperpolarization increases because of activation of the pre-catalyst removing the cyclooctadiene (COD) substituent and because of increased availability of *p*-H_2. The threshold of polarization to induce RASER effects is crossed after a polarization buildup and activation period of 340 s. The signal in Fig. 6b is initialized with a 90-degree proton pulse to open the receiver channel on the spectrometer. While the 90-degree pulse uses up most of the magnetization in the sensitive volume, this volume is displaced in 3.0 s at a pumping rate of 2.0 mL/min. Notably, as the polarization increases above the RASER threshold, the buildup time for observation of the emitted RASER pulses after the 90-degree pulse shortens significantly as the system reaches a higher polarization level.

In the presented RASER experiments with the STAR system, we use a minimal 2-degree initialization pulse as limited by the NMR spectrometer [51] to open the receiver channel. As depicted in Fig. 7a, we detect a continuous RASER signal for 157.2 s in the Spinsolve system, limited in our detection time only by the single experiment data acquisition memory of the spectrometer. For these extended acquisition periods the number of points acquired in the time domain is maximized to the memory limit by increasing the dwell time close to

the Nyquist sampling limit. However, even in this almost under sampled case we observe continuous RASER signal for the entire acquisition period.

As a first simple demonstration of an application, the continuous acquisition allows for an accurate measurement of the magnetic field drift of the permanent magnet array. In Figure 7(c), a simple quadratic polynomial is fit to the drifting NMR frequency. The fitting procedure is carried out on a sliced time domain, described in further detail in SI section 9.1. After correction of the quadratic drift, we obtain a single NMR peak for pyrazine, as all protons in the chemical system are equivalent. The Fourier transform (FFT) NMR peak has a full width half maximum (FWHM) linewidth of 7.7 mHz equal to the theoretical minimum, based on the total acquisition time of the RASER (157.2 s). The theoretical minimum is calculated by taking the Fourier transform of a general rectangular function with L=157.2 s. The details of this calculation and comparison including the mathematical analysis of the full rectangular window are provided in SI section 9.3.

Furthermore, we demonstrate the detection of continuous RASER signal from a pyrazine SABRE solution continuously detected at 9.4 T for 1000 s (Fig. 7(e)). The acquisition of the RASER at 9.4 T does not use an initialization pulse as in the 1.1 T case above, however relaxation oscillations in the RASER buildup [52] are still observed at the beginning of the acquisition period. They are initiated by the internal electronics of the Bruker probe that opens the LC resonator completing the RASER circuit when acquisition is started. The magnitude FFT of the RASER FID is shown in Figure 7(f). In this RASER spectrum, we observe many lines despite only the single proton species in the pyrazine molecule. The appearance of the multiple equidistant features (frequency comb) is due to the pulsatile pumping rate of hyperpolarized solution into the NMR tube. The substructure within each line of the frequency comb is a result of chaotic mixing as the solution is injected into the NMR tube. Both effects (frequency comb and substructure) are caused by distant dipolar fields generated by the hyperpolarized spin system that in turn shifts the resonance frequencies. We note that related frequency comb effects are also visible in the in the 1.1 T RASER at a lower magnitude, with a separation frequency of 1.42 Hz (See SI Section 10).

Based on the present demonstrations, the STAR system is well positioned to be expanded in future studies for both high- and low-field RASER experiments, including heteronuclear RASER phenomena by coupling the continuous SABRE-SHEATH approach described above to high Q resonant circuits.

Conclusion

The STAR system represents an addition to parahydrogen instrumentation, which enables continuous hyperpolarization that can be coupled to many magnetic resonance applications. In the present work, we highlight the utility of the STAR for various SABRE-based parahydrogen experiments. First, continuous proton SABRE is demonstrated on pyridine and pyrazine, detected at 1.1 T and 9.4 T. This is followed by the demonstration of continuous heteronuclear SABRE-SHEATH on $^{15}N_3$ metronidazole detected at 9.4 T and $^{13}C_2$ pyruvate detected at 1.1 T. Finally, the detection of decay-free NMR signal is demonstrated by exploiting the SABRE-pumped RASER with pyrazine at 1.1 T and

9.4 T. At 1.1 T the theoretically highest resolution with an acquisition time of 157.2 s acquisition time is obtained, whereas at 9.4 T, with a different flow cell, RASER effects that cause frequency combs and chaotic behaviors are observed. These examples emphasize the highly modular nature of the system, allowing for simple adaptation of the continuous SABRE hyperpolarization to any nucleus and any detection system. It is also important to bear in mind the compact nature of the STAR with a footprint of less than 30×50 cm^2, which makes it portable and quickly adaptable in new environments. experiment. Ongoing further optimization of the gas delivery is also possible with full characterization and modelling of the gas transfer characteristics. Compared to previous continuous implementations of SABRE with bubbling setups, the STAR has highly reduced solvent evaporation allowing for operation for many hours making this hyperpolarization approach compatible with any standard multidimensional NMR. The current mode of operation may lend itself to advanced hyperpolarization studies with fast averaging and multidimensional experiments for exploration of protein interactions with hyperpolarized ligands or solvent. The work can also be geared towards *in vivo* imaging with parahydrogen hyperpolarization, taking advantage of the continuous production of hyperpolarized substrates for continuous metabolic imaging under steady state metabolic conditions. Moving forward, the presented work can also be adapted to rapid hydrogenative PHIP experiments. Finally, the current work also lays a foundation for future explorations of RASER physics, multi-mode effects at multi-Tesla fields, or the exploration of heteronuclear RASER systems at any target magnetic field. Given the straightforward adaptation to any magnet or magnetic field, we envision several STAR-RASER application, including high precision measurement of Earth's magnetic field rotation with a RASER-based gyroscope [33]

Supplementary Material

Refer to Web version on PubMed Central for supplementary material.

Acknowledgements

Acknowledgements Text. Research reported in this publication was supported by the National Institute of Biomedical Imaging and Bioengineering of the National Institutes of Health under Award Numbers NIH R21-EB025313 and NIH R01EB029829. The content is solely the responsibility of the authors and does not necessarily represent the official views of the National Institutes of Health. In addition, we acknowledge funding from the Mallinckrodt Foundation, the National Science Foundation under award NSF CHE-1904780, and from the National Cancer Institute under award number NCI 1R21CA220137, as well as funding from the North Carolina Biotechnology Center in the form of a Translational Research Grant.

References

[1]. Halse ME, TrAC - Trends Anal. Chem 2016, 83, 76–83.

[2]. Kovtunov KV, Pokochueva EV, Salnikov OG, Cousin SF, Kurzbach D, Vuichoud B, Jannin S, Chekmenev EY, Goodson BM, Barskiy DA, Koptyug IV, Chem. - An Asian J 2018, 13, 1857–1871.

[3]. Goldman M, Abragam A, Reports Prog. Phys 1978, 41, 395.

[4]. Walker TG, Happer W, Rev. Mod. Phys 1997, 69, 629–642.

[5]. Bowers CR, Weitekamp DP, Phys. Rev. Lett 1986, 57, 2645–2648. [PubMed: 10033824]

[6]. Hovener J, Pravdivtsev AN, Kidd B, Bowers CR, Glöggler S, V Kovtunov K, Plaumann M, Katz-Brull R, Buckenmaier K, Jerschow A, Reineri F, Theis T, V Shchepin R, Wagner S,

Zacharias NMM, Bhattacharya P, Chekmenev EY, Angew. Chemie Int. Ed 2018, DOI 10.1002/anie.201711842.

[7]. Adams RW, Aguilar JA, Atkinson KD, Cowley MJ, Elliott PIPP, Duckett SB, Green GGRR, Khazal IG, Lopez-Serrano J, Williamson DC, Science (80-.). 2009, 323, 1708–1711.

[8]. Nikolaou P, Goodson BM, Chekmenev EY, Chem. - A Eur. J 2015, 21, 3156–3166.

[9]. Adams RW, Duckett SB, Green RA, Williamson DC, Green GGRR, J. Chem. Phys 2009, 131, 194505. [PubMed: 19929058]

[10]. Barskiy DA, Knecht S, Yurkovskaya AV, Ivanov KL, Prog. Nucl. Magn. Reson. Spectrosc 2019, 114–115, 33–70.

[11]. Richardson PM, Jackson S, Parrott AJ, Nordon A, Duckett SB, Halse ME, Magn. Reson. Chem 2018, 56, 641–650. [PubMed: 29193324]

[12]. Duckett SB, Mewis RE, Acc. Chem. Res 2012, 45, 1247–1257. [PubMed: 22452702]

[13]. Lehmkuhl S, Wiese M, Schubert L, Held M, Küppers M, Wessling M, Blümich B, J. Magn. Reson 2018, 291, 8–13. [PubMed: 29625356]

[14]. Štěpánek P, Sanchez-Perez C, Telkki V-V, Zhivonitko VV, Kantola AM, J. Magn. Reson 2019, 300, 8–17. [PubMed: 30684826]

[15]. Roth M, Kindervater P, Raich HP, Bargon J, Spiess HW, Münnemann K, Angew. Chemie - Int. Ed 2010, 49, 8358–8362.

[16]. Hale WG, Zhao TY, Choi D, Ferrer M, Song B, Zhao H, Hagelin-Weaver HE, Bowers CR, ChemPhysChem 2021, 22, 822–827. [PubMed: 33689210]

[17]. Yang L, Jensen KF, Org. Process Res. Dev 2013, 17, 927–933.

[18]. Ramezani M, Kashfipour MA, Abolhasani M, J. Flow Chem 2020, 10, 93–101.

[19]. Han S, Kashfipour MA, Ramezani M, Abolhasani M, Chem. Commun 2020, 56, 10593–10606.

[20]. Yue J, Chen G, Yuan Q, Luo L, Gonthier Y, Chem. Eng. Sci 2007, 62, 2096–2108.

[21]. Mallia CJ, Baxendale IR, 2016, DOI 10.1021/acs.oprd.5b00222.

[22]. Charpentier J-C, in Adv. Chem. Eng (Eds.: Drew TB, Cokelet GR, Hoopes JW, Vermeulen T), Academic Press, 1981, pp. 1–133.

[23]. Shchepin RV, Goodson BM, Theis T, Warren WS, Chekmenev EY, ChemPhysChem 2017, 18, 1961–1965. [PubMed: 28557156]

[24]. Colell JFP, Logan AWJ, Zhou Z, V Shchepin R, Barskiy DA, Ortiz GX, Wang Q, Malcolmson SJ, Chekmenev EY, Warren WS, Theis T, J. Phys. Chem. C 2017, 121, 6626–6634.

[25]. Serrao EM, Brindle KM, Front. Oncol 2016, 6, 1–6. [PubMed: 26858933]

[26]. Bok R, Vigneron DB, van Criekinge M, Reed G, Hurd RE, Chen AP, Nelson SJ, Park I, Larson PEZ, Ardenkjaer-Larsen JH, Robb FJ, Small EJ, Odegardstuen L-I, Munster P, Carvajal L, Weinberg VK, Kurhanewicz J, Tropp J, Murray JA, Chang JW, Harzstark AL, Ferrone M, Sci. Transl. Med 2013, 5, 198ra108–198ra108.

[27]. Shukla-Dave A, Hricak H, NMR Biomed. 2014, 27, 16–24. [PubMed: 23495081]

[28]. Barskiy DA, Shchepin RV, Coffey AM, Theis T, Warren WS, Goodson BM, Chekmenev EY, J. Am. Chem. Soc 2016, 138, 8080–8083. [PubMed: 27321159]

[29]. Ariyasingha NM, Lindale JR, Eriksson SL, Clark GP, Theis T, Shchepin RV, Chukanov NV, Kovtunov KV, Koptyug IV, Warren WS, Chekmenev EY, J. Phys. Chem. Lett 2019, 10, 4229–4236. [PubMed: 31291106]

[30]. Hu S, Balakrishnan A, Bok RA, Anderton B, Larson PEZ, Nelson SJ, Kurhanewicz J, Vigneron DB, Goga A, Cell Metab. 2011, 14, 131–142. [PubMed: 21723511]

[31]. Gallagher FA, Woitek R, McLean MA, Gill AB, Garcia RM, Provenzano E, Riemer F, Kaggie J, Chhabra A, Ursprung S, Grist JT, Daniels CJ, Zaccagna F, Laurent MC, Locke M, Hilborne S, Frary A, Torheim T, Boursnell C, Schiller A, Patterson I, Slough R, Carmo B, Kane J, Biggs H, Harrison E, Deen SS, Patterson A, Lanz T, Kingsbury Z, Ross M, Basu B, Baird R, Lomas DJ, Sala E, Wason J, Rueda OM, Chin SF, Wilkinson IB, Graves MJ, Abraham JE, Gilbert FJ, Caldas C, Brindle KM, Proc. Natl. Acad. Sci. U. S. A 2020, 117, 2092–2098. [PubMed: 31964840]

[32]. Suefke M, Lehmkuhl S, Liebisch A, Blümich B, Appelt S, Nat. Phys 2017, 13, 568–572.

[33]. Appelt S, Kentner A, Lehmkuhl S, Blümich B, Prog. Nucl. Magn. Reson. Spectrosc 2019, 114–115, 1–32.

[34]. Resnick PR, Buck WH, in Mod. Fluoropolymers (Ed.: Scheirs J), John Wiley & Sons, Ltd., 1997, pp. 397–419.

[35]. Ma L-C, Chen C, Lin JYS, Ind. Eng. Chem. Res 2020, 59, 16795–16804.

[36]. Theis T, Truong ML, Coffey AM, Shchepin RV, Waddell KW, Shi F, Goodson BM, Warren WS, Chekmenev EY, J. Am. Chem. Soc 2015, 137, 1404–1407. [PubMed: 25583142]

[37]. Ivanov KL, Pravdivtsev AN, Yurkovskaya AV, Vieth H-MM, Kaptein R, Prog. Nucl. Magn. Reson. Spectrosc 2014, 81, 1–36. [PubMed: 25142733]

[38]. Theis T, Ortiz GX, Logan AWJ, Claytor KE, Feng Y, Huhn WP, Blum V, Malcolmson SJ, Chekmenev EY, Wang Q, Warren WS, Sci. Adv 2016, 2, 1–8.

[39]. Cowley MJ, Adams RW, Atkinson KD, Cockett MCR, Duckett SB, Green GGR, Lohman JAB, Kerssebaum R, Kilgour D, Mewis RE, J. Am. Chem. Soc 2011, 133, 6134–6137. [PubMed: 21469642]

[40]. Rajendran JG, Wilson DC, Conrad EU, Peterson LM, Bruckner JD, Rasey JS, Chin LK, Hofstrand PD, Grierson JR, Eary JF, Krohn KA, Eur. J. Nucl. Med. Mol. Imaging 2003, 30, 695–704. [PubMed: 12632200]

[41]. Barskiy DA, Shchepin RV, Coffey AM, Theis T, Warren WS, Goodson BM, Chekmenev EY, J. Am. Chem. Soc 2016, 138, 8080–8083. [PubMed: 27321159]

[42]. Shchepin RV, Birchall JR, Chukanov NV, Kovtunov KV, Koptyug IV, Theis T, Warren WS, Gelovani JG, Goodson BM, Shokouhi S, Rosen MS, Yen Y, Pham W, Chekmenev EY, Chem. – A Eur. J 2019, 176, chem.201901192.

[43]. Gemeinhardt ME, Limbach MN, Gebhardt TR, Eriksson CW, Eriksson SL, Lindale JR, Goodson EA, Warren WS, Chekmenev EY, Goodson BM, Angew. Chemie - Int. Ed 2020, 59, 418–423.

[44]. Tickner BJ, Semenova O, Iali W, Rayner PJ, Whitwood AC, Duckett SB, Catal. Sci. Technol 2020, 10, 1343–1355. [PubMed: 32647563]

[45]. Iali W, Roy SS, Tickner BJ, Ahwal F, Kennerley AJ, Duckett SB, Angew. Chemie 2019, 131, 10377–10381.

[46]. Tickner BJ, Lewis JS, John RO, Whitwood AC, Duckett SB, Dalt. Trans 2019, 48, 15198–15206.

[47]. Cavallari E, Carrera C, Aime S, Reineri F, J. Magn. Reson 2018, 289, 12–17. [PubMed: 29448129]

[48]. Cavallari E, Carrera C, Sorge M, Bonne G, Muchir A, Aime S, Reineri F, Sci. Rep 2018, 8, 8366. [PubMed: 29849091]

[49]. Vuichoud B, Bornet A, de Nanteuil F, Milani J, Canet E, Ji X, Miéville P, Weber E, Kurzbach D, Flamm A, Konrat R, Gossert AD, Jannin S, Bodenhausen G, Chem. - A Eur. J 2016, 22, 14696–14700.

[50]. Patel CKN, Faust WL, McFarlane RA, Appl. Phys. Lett 1962, 1, 84–85.

[51]. Joalland B, Ariyasingha NM, Lehmkuhl S, Theis T, Appelt S, Chekmenev EY, Angew. Chemie - Int. Ed 2020, 59, 8654–8660.

[52]. Appelt S, Lehmkuhl S, Fleischer S, Joalland B, Ariyasingha NM, Chekmenev EY, Theis T, J. Magn. Reson 2020, 106815. [PubMed: 33423756]

[53]. Pravdivtsev AN, Sönnichsen FD, Hövener JB, ChemPhysChem 2020, 21, 667–672. [PubMed: 31898393]

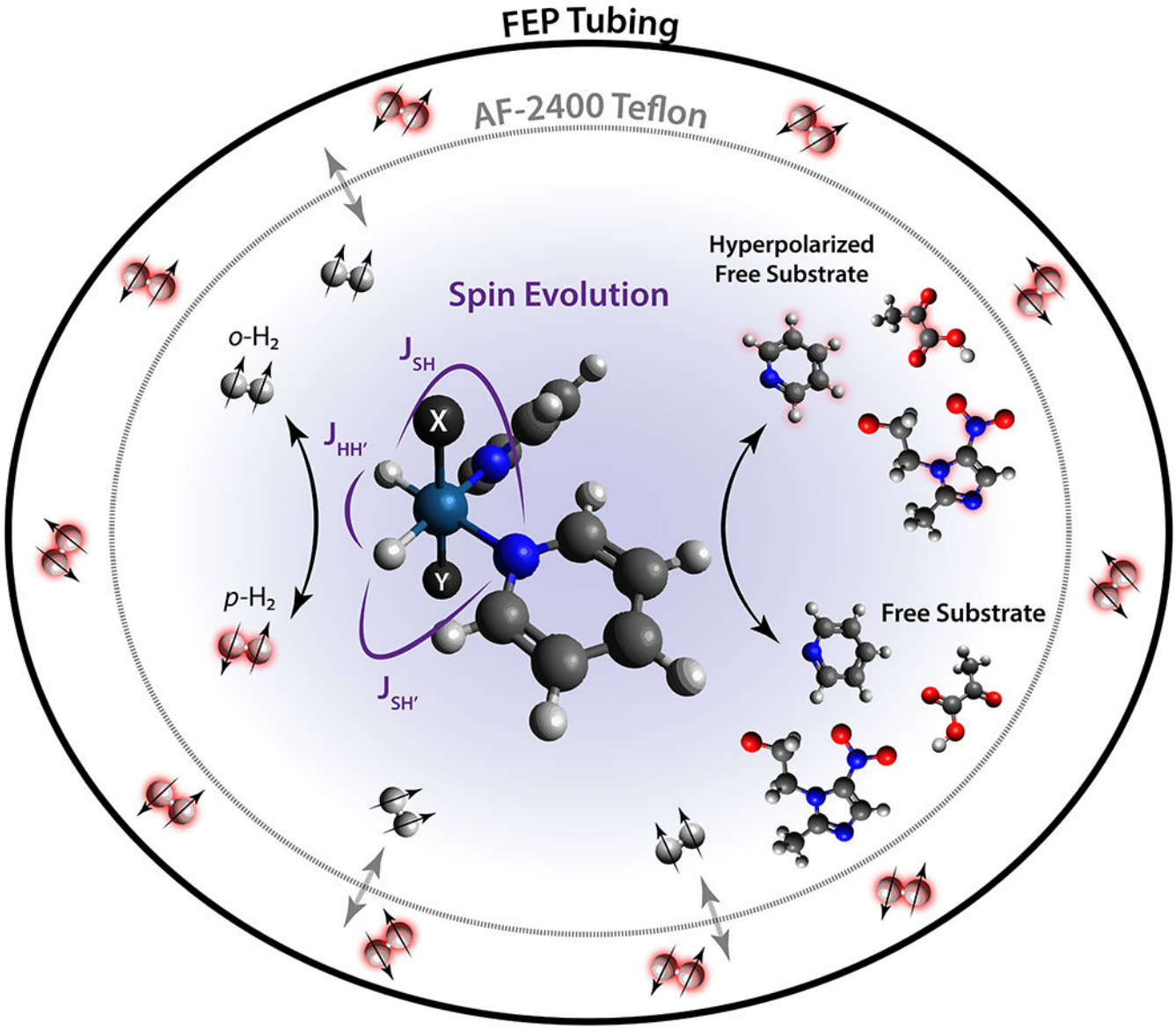

Figure 1.

Schematic of SABRE in a cross-section of the Spin Transfer Automated Reactor (STAR). Para and Ortho hydrogen exchange across the membrane occurs between the outer gas annulus and inner liquid annulus. Of the SABRE complex, only equatorial ligands are, where **X**=IMes (1,3 - bis(2,4,6 - trimethylphenyl) imidazole-2-ylidene) and **Y**=pyridine in the axial plane. The J-couplings represent the necessary scalar couplings for spin transfer from the para-hydrides to the target substrate.

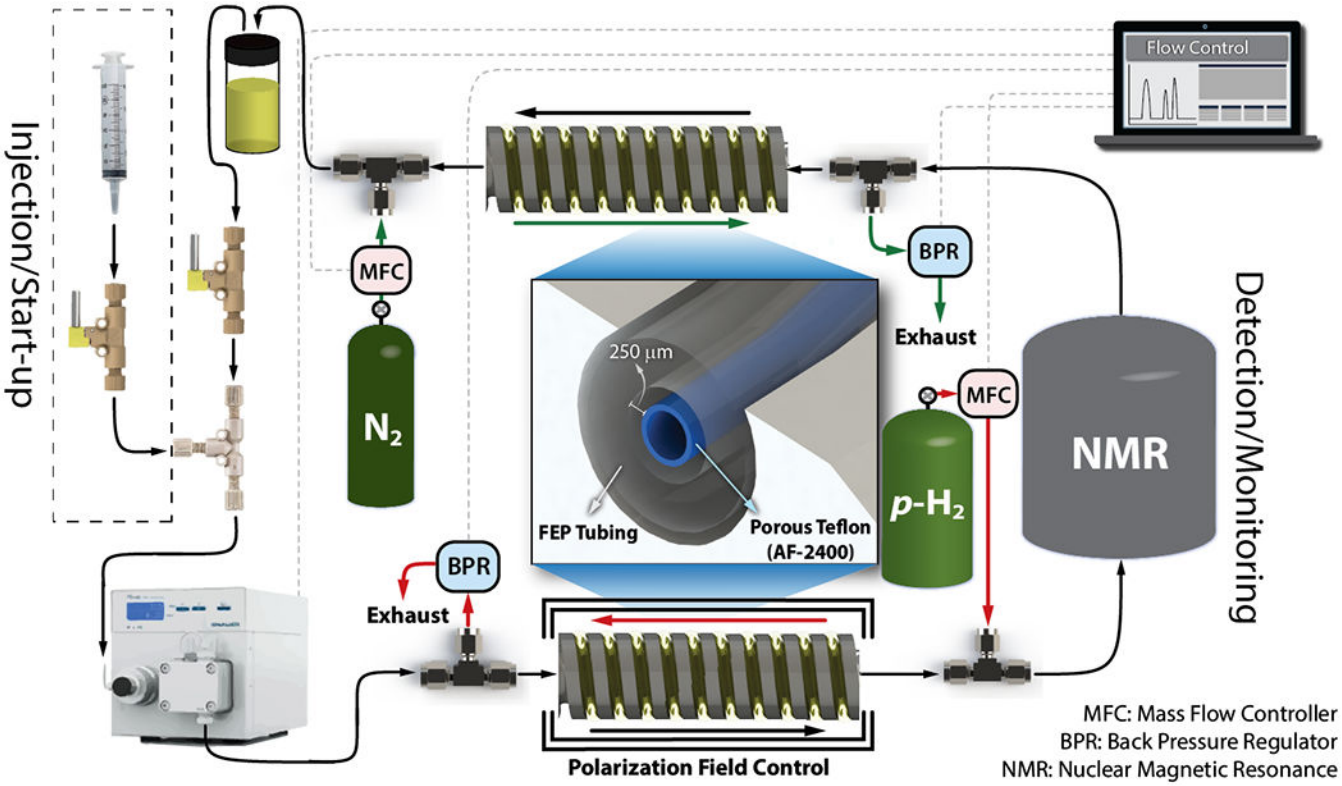

Figure 2.

Mode of operation of STAR, where a solution is injected into the fluid path and subsequently pumped in a closed loop, cycling through the pump, tube-in-tube reactors, benchtop NMR and system reservoir. In one standard configuration, the p-H_2 pressure is 100 psi and the N_2 pressure is 90 psi.

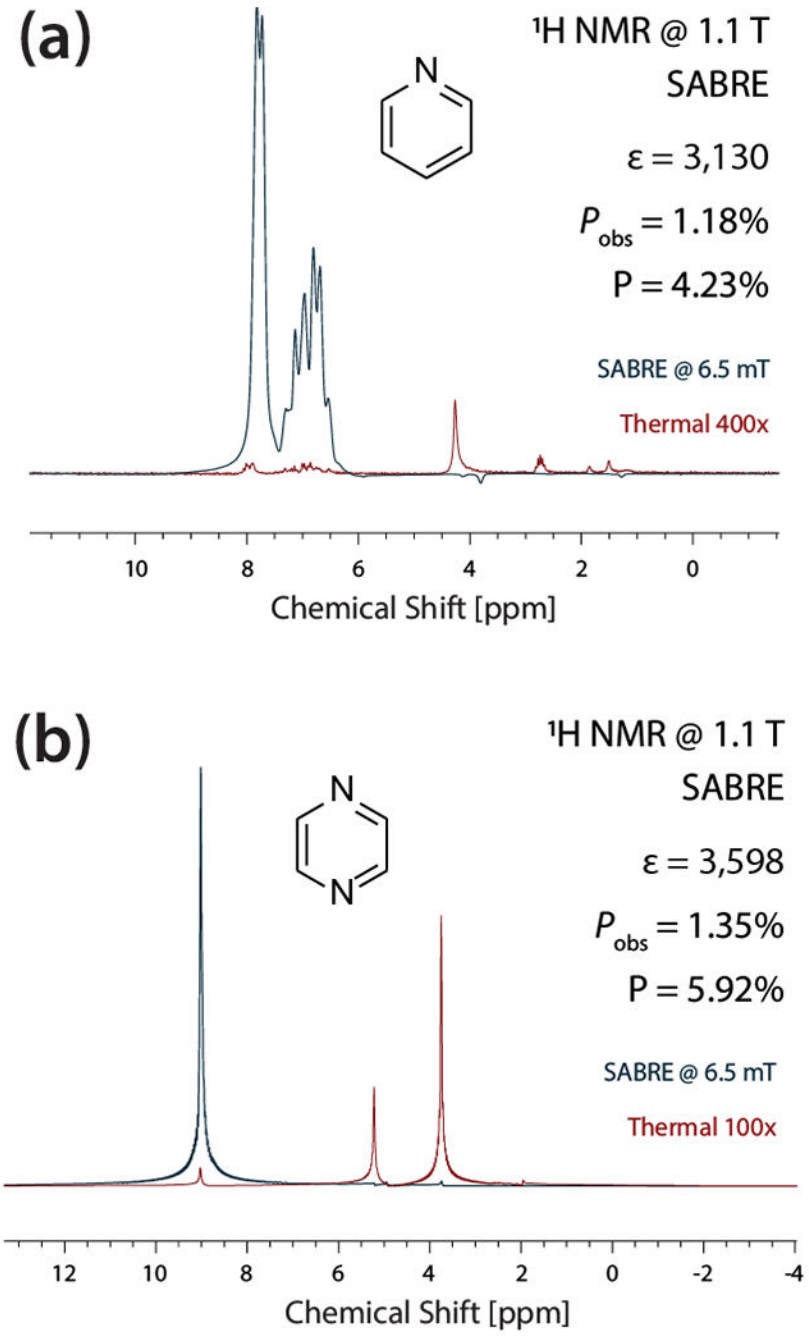

Figure 3.

Continuous STAR-SABRE polarization observed for both **(a)** pyridine and **(b)** pyrazine; sample composition for both spectra shown is 60 mM substrate + 3 mM IMes catalyst. Data is acquired in flow at 2 mL/min with p-H_2 pressure of 90 psi at 100 sccm. B_{pol}=6.5 mT.

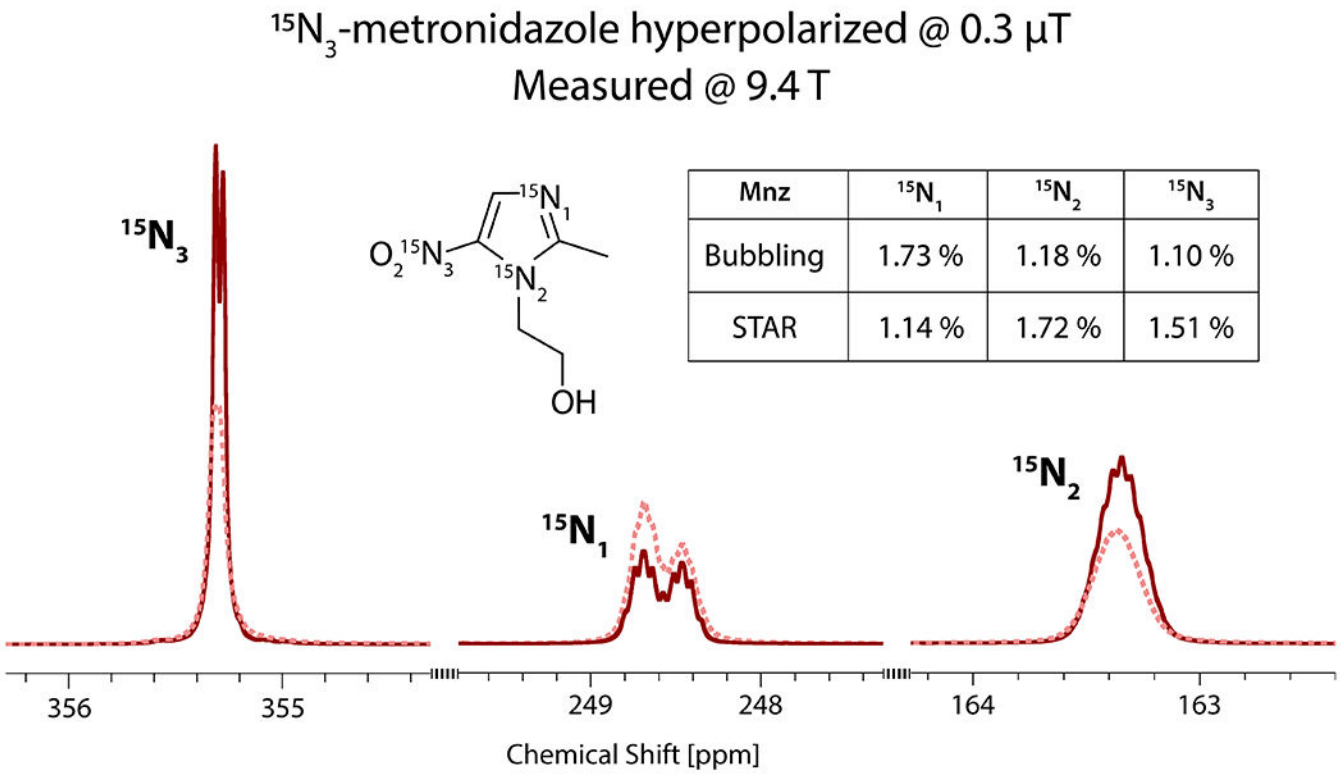

Mnz	$^{15}N_1$	$^{15}N_2$	$^{15}N_3$
Bubbling	1.73 %	1.18 %	1.10 %
STAR	1.14 %	1.72 %	1.51 %

Figure 4.

^{15}N hyperpolarization using SABRE-SHEATH in the STAR system. HP [$^{15}N_3$] metronidazole spectrum with the STAR system at 2.0 mL/min, 100 psi p-H_2 at 250 sccm. Light red overlay is the spectrum achieved with a standard bubbling mode. Sample composition for both spectra is 60 mM Mnz + 3 mM IMes catalyst. **Table** inset: Calculated polarization levels for each corresponding ^{15}N nuclei in metronidazole, based on [^{15}N] pyridine reference spectra (SI section 6).

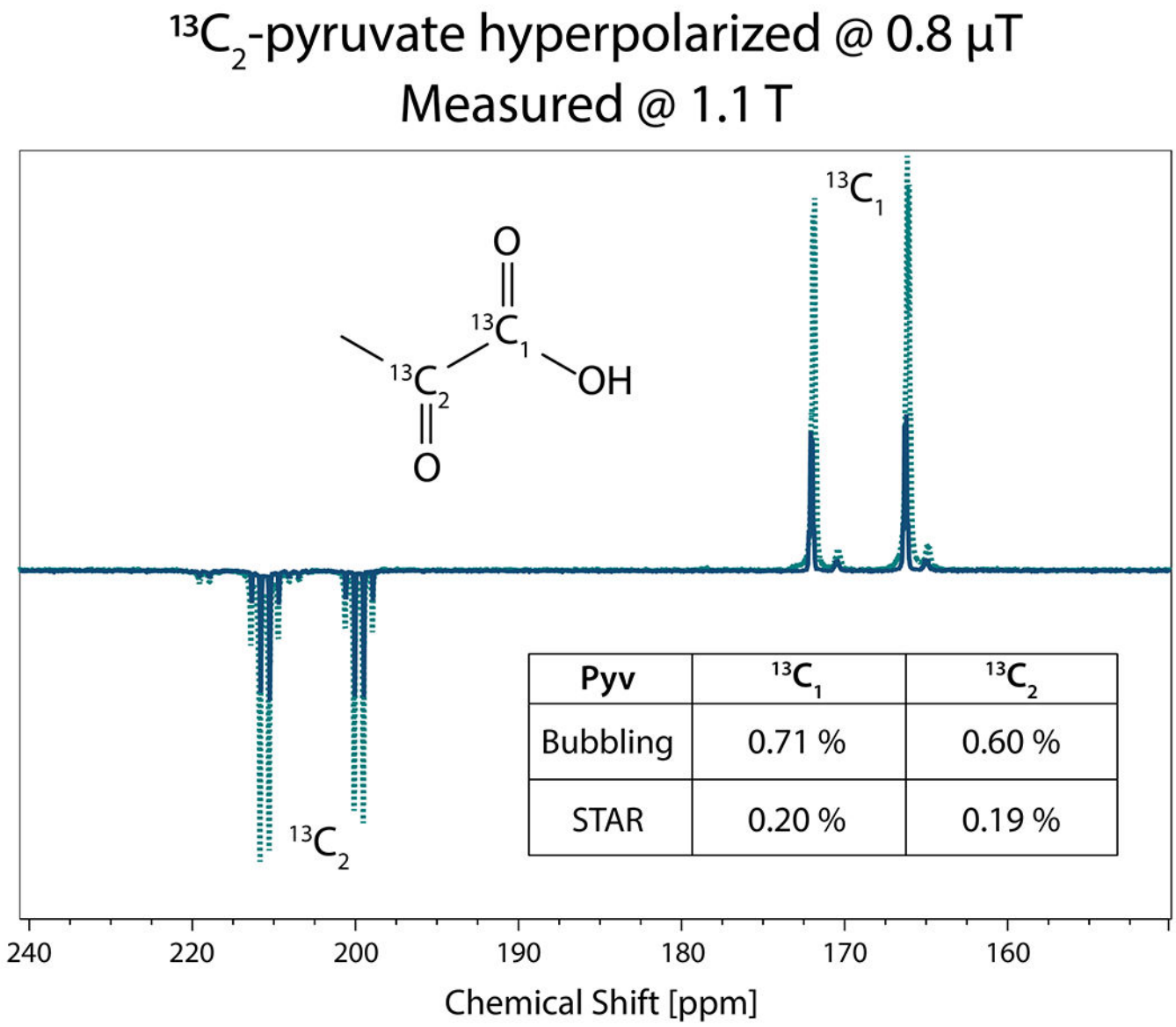

Figure 5.

^{13}C hyperpolarization using SABRE-SHEATH in the STAR system, detected at 1.1 T in a Magritek benchtop Spinsolve. Hyperpolarized [$^{13}C_2$]-pyruvate spectrum with the STAR system at 2 mL/min. Light blue overlay is the spectrum achieved with a standard bubbling mode. Sample composition for both spectra is 24 mM [$^{13}C_2$]-pyruvate + 30 mM DMSO + 3 mM IMes catalyst. **Table** inset: Calculated polarization levels for each corresponding ^{13}C nuclei in pyruvate, based on benzene the reference spectra (SI section 6).

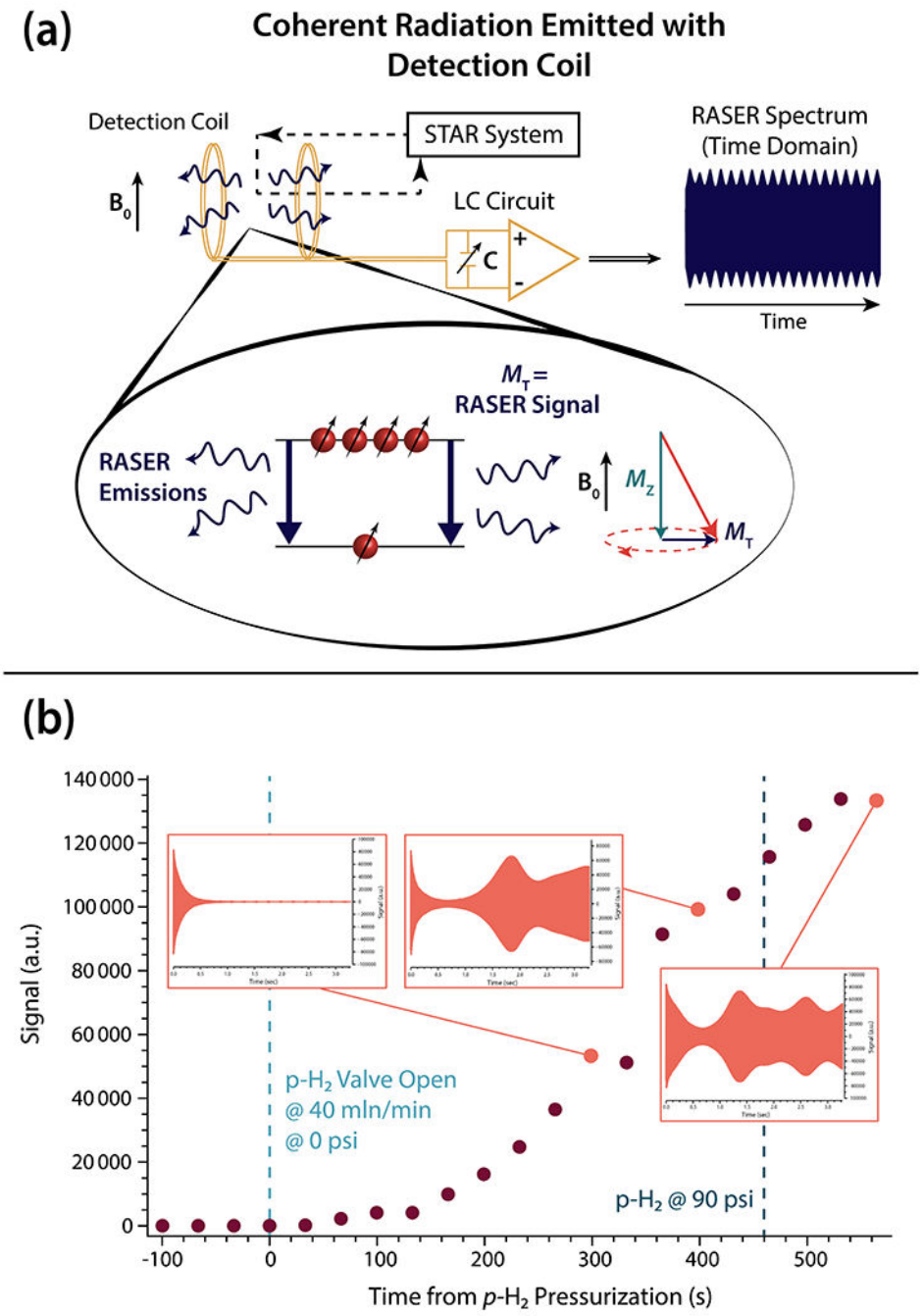

Figure 6.

RASER physics and corresponding results acquired with the STAR system. (**a**) Mode of operation of a RASER, where a continuously pumped polarized population inversion is coupled to photons in an NMR LC circuit. (**b**) Buildup of RASER effects observed where a RASER threshold is observed at ~0.5% polarization as the pressure is ramped from 0 to 90 psi. The FIDs shown inset are shown for an acquisition time of 3 s after a 90° initialization pulse, with the magnitude of each FID scaled for visualization of the relative time buildup of the RASER burst.

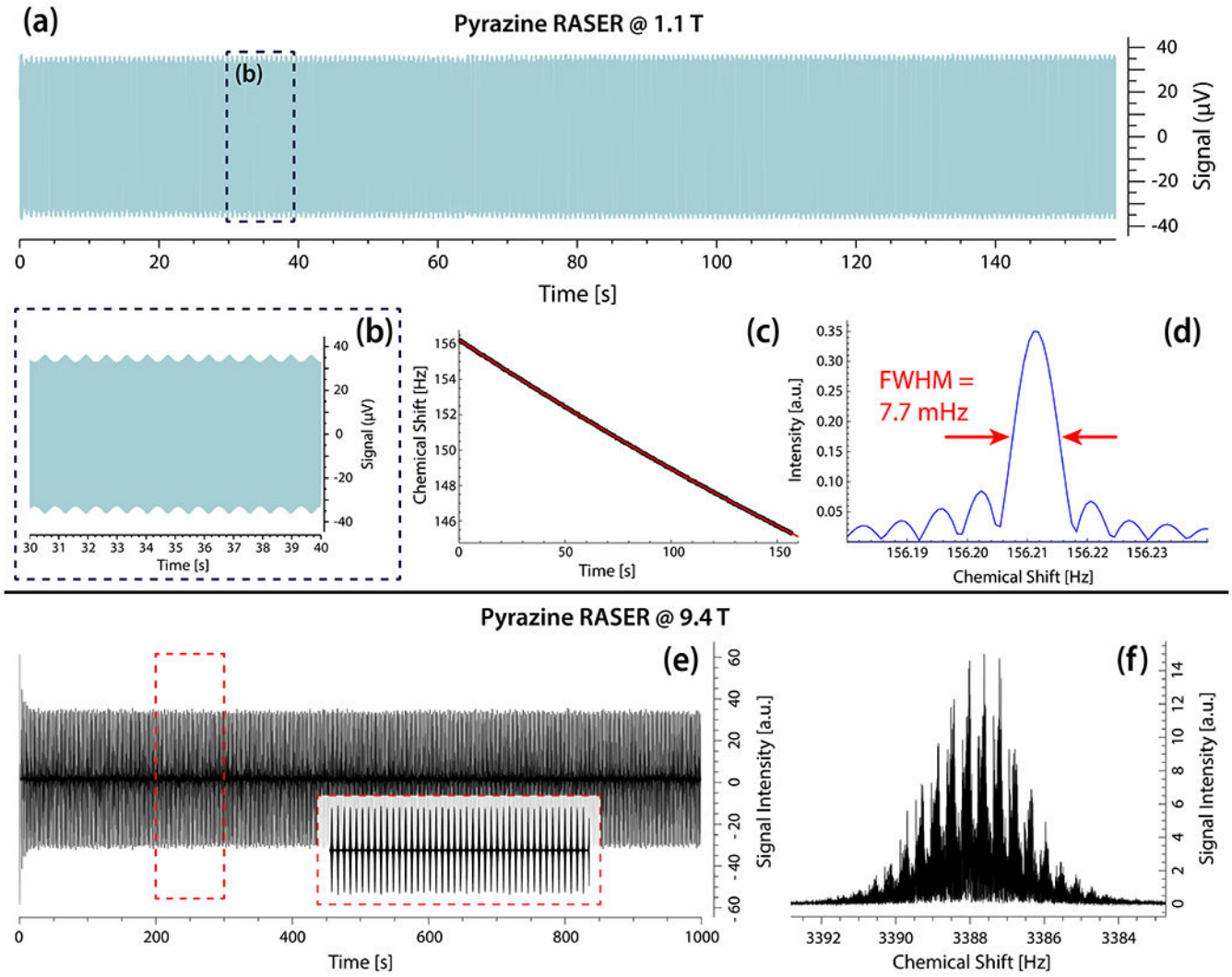

Figure 7.

Continuous RASER signal acquired with the STAR system at both 1.1 T and 9.4 T. In both cases the sample composition is 60 mM pyrazine + 3 mM IMes in CD_3OD. (**a-c**) 1.1 T pyrazine RASER (**a**) Continuous detection of a RASER from pyrazine protons with a total acquisition time of 157.3 s and a dwell time of 1200 μs. (**b**) Zoom of a single region of the pyrazine RASER time domain. (**c**) Calibration of the magnetic field drift using a quadratic fit and (**d**) corresponding drift-corrected Fourier transform of the full 157.2 s observed RASER, yielding the theoretically lowest possible FWHM of 7.7 mHz. (e-f) 9.4 T pyrazine RASER (e) Continuous detection of a RASER action with a total acquisition time of 1000 s, with an inset zoom of 100 s of the RASER time domain. (f) Corresponding FFT of the pyrazine RASER showing a frequency comb with a spacing of 0.42 Hz with chaotic substructure.